Journal of the Chinese Chemical Society, 1992, *39*, 511-527

Dynamics and Kinetics of Metal Atoms in the Gas Phase

King-Chuen Lin (林金全)
Department of Chemistry, National Taiwan University and Institute of Atomic and Molecular Sciences, Academia Sinica, Taipei, Taiwan 10764, R.O.C.

The review is divided into four sections. We first consider the varied behavior of K n^2S and n^2D states in their chemical reactivity and physical characterization. We review the effect of orbital alignment of an electronically excited metal atom on the cross section of energy transfer or chemical reaction, and report the technique of a single supersonic jet employed to measure this effect on the Ca spin-changing collision. We discuss the effects of temperature and isotopic mass on the distribution of rotational quantum number of the product MgH to identify the reaction mechanism of $Mg(^1P_1) + H_2$. The final concerns are the quantum yield, fine-structure branching ratio and rate of collisional mixing for the K ^2P_J doublets following photodissociation of KI at 193 nm.

In the light of the enormously abundant metallic elements on earth, their importance to our lives is beyond description. The associated dynamics or kinetics of the metallic atoms in the gas phase has long been investigated, and the subject is impossible to review completely in one article. We therefore confine the scope to topics closely related to our experiments, namely energy storage and depletion, effects of orbital alignment, reaction mechanism and photodissociation of diatomic molecules.

PROCESSES OF ENERGY STORAGE AND DEPLETION

Although the first few excited states of alkali atoms in collisions with H_2 have been extensively investigated, there is still lacking a clear understanding of various aspects of their dynamic behavior. For instance, a controversy exists about the reaction mechanism of Cs*(7P) with H_2 at the threshold energy.[1-4] Sayer et al. proposed that the subsequent CsH product results from a multistep-collision mechanism, and that the reaction rate depends on the ground-state population of Cs(6S);[1,2] either H_2 in a highly excited vibrational level or the CsH_2 complex is involved as an intermediate. In contrast, Vetter et al. using a crossed-beam apparatus demonstrated that a single collision leads to the reaction product CsH;[3,4] they suggested that the harpoon mechanism plays a dominant role in the reaction, of which the reactants correlate symmetrically with the ion-pair complex Cs^+HH^-, a collinear configuration as an intermediate, and then correlate with the products. In an attempt to clarify this ambigious situation, we investigated a similar reaction involving excited K atoms with H_2 molecules. However, our reaction is initiated from metastable states of 7S and 5D and of greater exothermicity. The large excess energy makes it possible to examine the coupling of the partitioning between rotational and vibrational energy, which may be conducive to an understanding of the orientation of the reactants in the approach to a reactive encounter.

We employed a pump-and-probe technique to monitor the resultant laser-induced fluorescence (LIF) of KH in a reaction heat-pipe oven operated at 470 K.[5] The pump beam using DCM as laser dye emitted at a wavelength about 660 nm, to prepare the potassium population in either 7S or 5D states by two-photon absorption. With coumarin 500 dye, a probe laser in counter propagation radiated in the range of wavelengths 500-510 nm, to monitor the LIF of the subsequent KH product. The probe beam was spatially delayed 5-8 ns, during which the fraction of nascent KH product encountering secondary collisions by H_2 molecules was negligible as the total pressure was maintained less than 10 Torr.

After K was excited to the 5D state with the pump laser, the probed LIF signal of (5,0)R5 line of the KH transition ($A^1\Sigma^+ - X^1\Sigma^+$) (Fig. 1a) was buried in the stray light, which was produced when either pump or probe beam passed through the heat-pipe oven. The reaction of K*(5D) with H_2 occurs to an evidently unmeasurable extent. In contrast, excitation of K*(7S) by two-photon absorption leads to a remarkable amount of LIF on the (5,0)R5 rotational line detected under otherwise the same conditions (Fig. 1b). By measuring the atomic LIF signal on the K(7S-4P) and K(5D-4P) transition, and taking into

This review is invited to commemorate the sixtieth anniversary of the Chinese Chemical Society.

account the spontaneous emission coefficients for the respective transitions, we estimate the population density of K*(7S) about one fifth that of K*(5D). The results also indicate a ratio 1/5 for the two-photon excitation cross sections to these two states. The difference in energy between the 5D state and the 7S state, 88 cm^{-1}, is much smaller than the value of kT = 330 cm^{-1}. Thus both reactions with H_2 molecules are exothermic by approximately 108 kJ mol^{-1}. Such a state-selective reaction was observed for the first time in the K*-H_2 system.[5] Analogously to this, Lee and coworkers demonstrated that the reaction product of NaO in a crossed-beam experiment was initiated by only the nD states of Na with O_2 molecule but not by the nP or nS states.[6] Reiland et al. have also found that NaO from the reaction of Na*(4D) with O_2 showed a significant alignment dependence.[7]

Although the K*(5D) atom releases an electron as easily as the K*(7S) atom, why is the KH product generated through the K*(7S), but not through the K*(5D)? We consider the problem from the viewpoint of symmetry correlation. We list in Table 1 the symmetry pattern for the system. Obviously K*(7S) + $H_2(X^1\Sigma_g^+)$ has the same symmetry as the collinear ion-pair complex K^+HH^- and the product $KH(X^1\Sigma^+)$ + $H(^2S_{1/2})$. Nevertheless, when the K*(5D) and

Table 1. Symmetry Correlation

	Symmetry		
System	$C_{\infty v}$	C_s	C_{2v}
$K(7s^2S)$ + $H_2(X^1\Sigma_g^+)$	Σ^+	A′	A_1
$K(5d^2D)$ + $H_2(X^1\Sigma_g^+)$	Σ^+	3A′	$2A_1$
	2Π	2A″	A_2
	2Δ		B_1
			B_2
$K^+(^1S)$ + $H_2^-(^2\Sigma_u^+)$	Σ^+	A′	A_1
$KH(X^1\Sigma^+)$ + $H(1s^2S)$	Σ^+	A′	A_1

the H_2 approach collinearly, the potential energy surface splits into three states Σ, Π and Δ. The population distributed statistically in the Σ state takes at most a fraction of 1/5. In addition, the surface is repulsive, for the electronic clouds overlap between the atomic d_z^2 orbital and the σ orbital;[8] thus the collision between K*(5D) and H_2 along the surface of Σ^+ appears much difficult. Only by Σ symmetry can the reactants initiated from K*(5D) correlate with the products. Such a harpoon mechanism may well account for our reaction, as the small ionization energy of K*(7S) facilitates release of an electron, thus leading to formation of a collinear ion-pair intermediate K^+HH^-. Two factors make unfavorable the formation of a bent complex K^+HH^-.

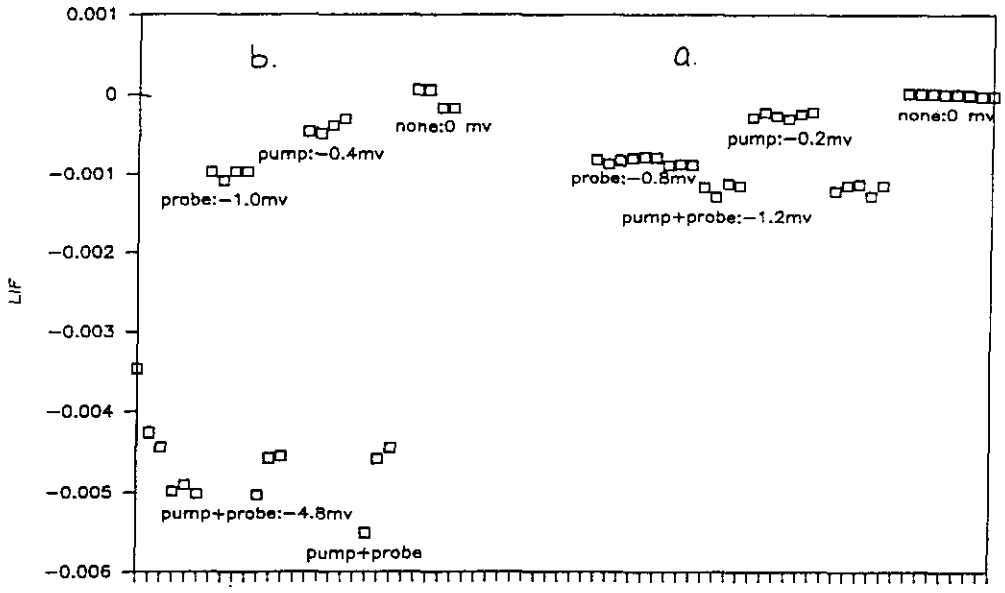

Fig. 1. Comparison of LIF signal probed on the (5,0)R5 rotational line of KH (A-X) transition. The pump laser was fixed at wavelength ~ 660 nm to prepare the states of K*(5D) or K*(7S) in the mixture with H_2 gas. A probe laser, with 5-8 ns spatially delayed, was used to monitor the yield of KH product. (a) KH produced from the reaction of K*(5D) with H_2; (b) KH produced from the reaction of K*(7S) with H_2. "none" indicates the baseline of LIF without irradiation of either laser; "pump" means LIF was obtained using the pump laser alone; "probe" means LIF was obtained using the probe laser alone; "pump+probe" means LIF was obtained using the pump-and-probe technique. Each sample point was averaged over 300 shots of laser pulses.

Compared to the high rotational energy levels of KH, (Fig. 2) the intensities for the low rotational energy distribution in general appear stronger; such a distribution indicates that a collinear collision prevails, for the energy transfer in the form of rotation is less significant. Secondly, the fractions of population located statistically in A′ and A_1 are 3/5 and 2/5 respectively, which make the chemical reaction via K*(5D) more feasible; in fact, we detected no LIF of KH from the 5D state.

Assuming that the ionic potential for the ion-pair intermediate in the long-range region may be attributed to coulombic attraction and ion-induced dipole interaction, the crossing region between the ionic potential surface and the covalent potential surface is located about 4.1-4.8 Å, which is still in the long-range attractive portion.[8] According to Landau-Zener theory, the channel for K*(7S) with H_2 should suffer the least barrier of potential energy to form the KH product. Experimentally, in the atomic LIF measurement on the K(7S-4P) transition at 579 nm, the collisional deactivation rate coefficient obtained as a function of temperature varies only slightly with increasing temperature. According to the Arrhenius theory, the activation energy for the reaction should be $< (12 \pm 4)$ kJ mol^{-1}, corresponding to a value 2-3 kT. This small barrier is consistent with the harpoon mechanism.

As the chemical reactivities of these two states appear distinct, their physical quenching properties are pertinent. We treated the deactivation of K(7^2S) or K(5^2D) atoms by gaseous H_2 using a three-level model of rate equations.[9] The time evolution of population density of K(7^2S) and K(5^2D) followed a bi-exponential function. In the early part of the decay, the population of the K(7^2S) is simply dominated by the two-photon excitation and the decay curve provides information on the effective lifetime of the K(7^2S) state by H_2 collisions. After prolonged delay the additional part of the K(7^2S) population contributed from the K(5^2D) state and possibly other states becomes important, but the rise time may be slow due to the delay caused by the migration between the two states. Accordingly we determine the effective lifetime by taking the portion within the early period with a slight correction from the long-time decay curve. As exemplified in Fig. 3 for the semi-log plot of the time-resolved fluorescence across the $7^2S - 4^2P_{1/2}$ transition with gaseous H_2 at pressure 0.04 torr, the slope obtained in the early decay yields a lifetime 110 ns, consistent with the result 111 ns obtained by computer simulation. The depopulation lifetime of the K(5^2D) state by collisions with H_2 is treated analogously.

Based on the Stern-Volmer equation, the plot of reciprocal effective lifetime as a function of H_2 pressure yields a slope indicating the deactivation cross section and an intercept indicating the radiative lifetime in the absence of H_2. The results are listed in Table 2. The radiative lifetime of K(7^2S) and K(5^2D), yielding (155 ± 8) ns and (561

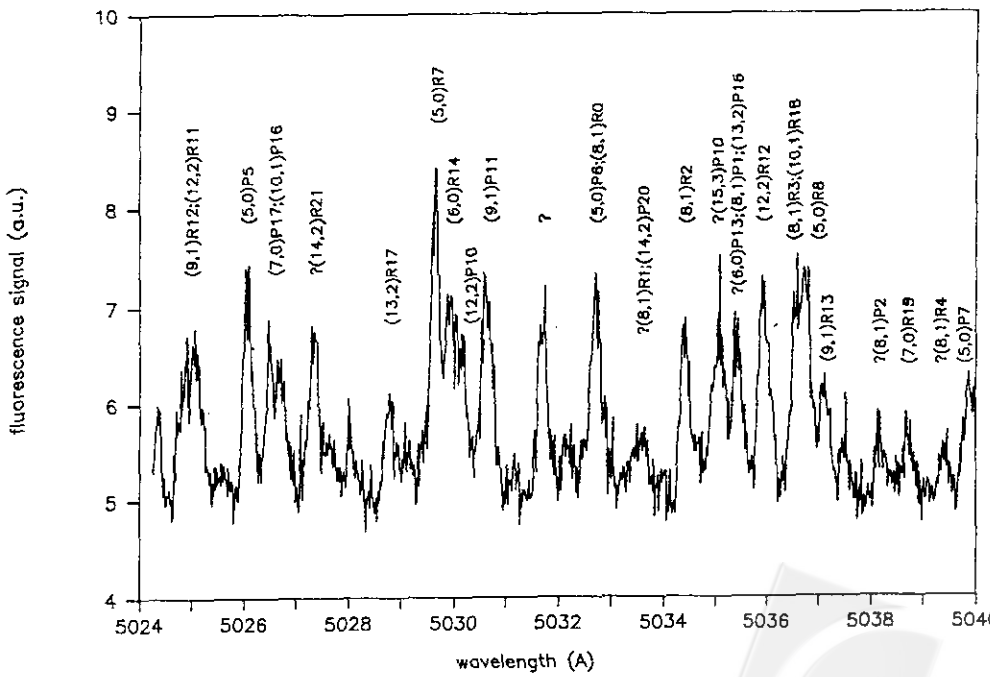

Fig. 2. A portion of nascent LIF spectrum of KH on A-X transition. Conditions: H_2 gas = 5 Torr, T = 470 K and delayed interval = 5 ns between pump and probe lasers.

Table 2. Radiative Lifetimes and Total Cross Sections for Deactivation by H_2 of K n^2S(n = 7-11) and n^2D(n = 5-8) States

	Lifetime (ns)					Cross section (Å2)
	This work	Others				This work
7^2S	157(5)[a]	165(12)[b]	157.8-152.8[c]	160[d]	160[e]	150(2)[a]
8^2S	227(16)	260(14)[b]	259.6-244.9[c]	269.2[d]	270[e]	167(5)
9^2S	391(32)	441(18)[b]	396.1-366.6[c]	423.4[d]	420[e]	189(9)
10^2S	562(41)	600(13)[b]	571.2-519.8[c]	628.3[d]	620[e]	208(17)
11^2S	803(57)	910(12)[b]	788.3-706.9[c]	895.4[d]	870[e]	231(27)
5^2D	569(12)[a]	610(90)[b]	749-692[c]	720[d]	710[e]	39(4)[a]
6^2D	798(32)	890(60)[b]	1087-943[c]	1066[d]	105[e]	26(4)
7^2D	1269(42)	1210(100)[b]	1390-1169[c]	1416[d]	1500[e]	28(3)
8^2D	1579(73)	1590(130)[b]	1742-1440[c]	1844[d]	1910[e]	20(2)

[a] see Ref. 9. [b] see Ref. 21. [c] see Ref. 10, temperature range 355-600 K.
[d] see Ref. 11. [e] see Ref. 12.

± 18) ns respectively, are found to coincide with the theoretical counterparts and those reported experimentally.[10-12] The cross sections for the K(7^2S) and K(5^2D) states are much larger than those of K 5^2P(12 Å^2) and 4^2P(3 Å^2) states. The K(7^2S) and K(5^2D) atoms bind weakly the outer-shell electron, thus having a large size. The average radii of K atoms in both the 7^2S and 5^2D states are approximately 18 Å, corresponding to an upper limit of the cross section 1000 Å^2 on a hard-sphere model.

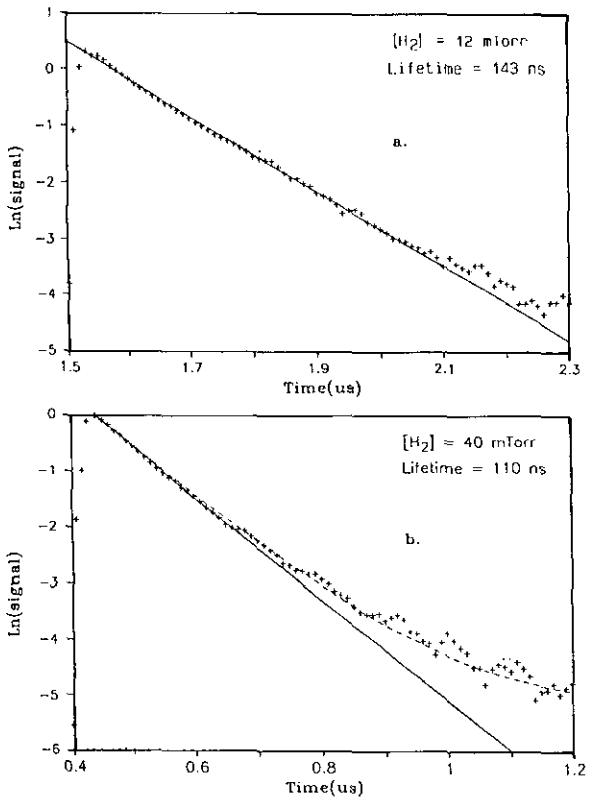

Fig. 3. Time-resolved fluorescence for the K atom in the 7^2S-$4^2P_{1/2}$ transition. (a) The pressure of H_2 is 12 mTorr and the effective lifetime is 143 ns; (b) the pressure of H_2 is 40 mTorr and the effective lifetime is 110 ns. A computer simulation of the decay curve is expressed as a dashed line, giving the effective lifetime of 111 ns.

A model of an electron harpoon accounts for the large quenching cross sections of molecular partners. According to this model, the cross section is expressed

$$\sigma = f\pi r_c^2, \quad (1)$$

where r_c is the ionic-covalent crossing radius; f denotes the fraction of covalent surfaces resulting from each excited atomic state that correlates with the ionic surface. For a transition structure of C_{2v} symmetry, f = 1 for the 7^2S states and f = 0.4 for the 5^2D states.[5] Thus the cross sections for deactivation of the 7^2S and 5^2D states are predicted to be (77 ± 29) and (31 ± 12) Å^2, respectively. As the values of electron affinity of H_2 and the effective polarizability are inaccurate,[13] the calculated values are only roughly compared to the experimentally derived values.

As the high-lying states of alkali atoms have varied properties such as effective size, polarizability and reactivity, their behaviors are characterized differently from those in the low-lying states.[14] The atoms in these states having an outer, loosely bound electron behave in a reaction more like an ion. Thus the model based on the free electron-perturber interaction (also called the impulse approximation) has been commonly employed, without correction for the ionic-core effect, to describe successfully the processes of energy depletion and change of angular momentum during collisions.[15,16] In this sense, an understanding of the reactivity of these states toward a collision partner may provide insight into correlation with the ion-molecule reaction. We have therefore extended the studies on deactivation of the excited K atom by H_2 to its moderate-

ly high-lying states.[17] The K n^2S (n = 8-11) or n^2D (n = 6-8) states are populated by a two-photon excitation. The effective lifetime of the K n^2S and $(n-2)^2D$ states in the presence of H_2 has been measured as described above. Based on the Stern-Volmer equation, Figs. 4 and 5 show the resulting plots for the cases of K n^2S (n = 8-11) and n^2D (n = 6-8) states. The results for the radiative lifetimes and the total cross sections for deactivation by H_2 appear in Table 2.

For the n^2S states, because the ionic core binds weakly the outer-shell ns electron, the effective size of these highly excited atoms and their subsequent collisional cross sections increase with increasing n. An alternative interpretation is by the model of electron harpoon. Because the curve-crossing region between the attractive ionic surface and the repulsive covalent surface moves towards a larger interparticle distance with increasing n, the deactivation cross section increases.[18,19] According to the harpoon model with symmetry correlation taken into account, the deactivation cross sections for the $(n-2)^2D$ states are smaller than those for the n^2S states. However, this simple model fails to explain the n dependence of the cross sections observed for the n^2D states.

Gallagher et al. have measured the collisional mixing cross sections on the order of 1000 $Å^2$ of highly excited Na(n^2D) with $l > 2$ states using noble gases, N_2 and CO as collision partners.[20,21] The collisional mixing is so rapid that the observed lifetime of n^2D corresponds to the average lifetime of all $l \geq 2$ states of the same n. Because the collision-induced mixing of the orbital angular momentum is so rapid, the total cross section of deactivation measured for the n^2D state is closely related to the manifold of $l \geq 2$ states of the same n. According to the harpoon model, the exit channel that removes the energy after a collision passes three or four potential curves at most. The effective rate of quenching therefore depends on the competition between the manifold and the lower atomic states for the exit channels. As the quantum number n increases, the energy separation between different $l \geq 2$ states becomes smaller. Thereby more states with $l \geq 2$ become involved in the mixing, and their mixing inside the manifold also becomes more rapid. Therefore, as suggested by Gallagher et al.,[20] the more states are included in the manifold as n icreases, the less effective the deactivation process becomes. This behavior qualitatively explains the n dependence of cross section for the n^2D states.

In relation to the rate of energy transfer from K n^2S to the closest $(n-2)^2D$ state, the 7^2S-5^2D specific transfer rate caused by H_2 collisions serves as an example. Its value is determined by comparison of a three-level model with the measurement of the H_2 pressure dependence of the integrated fluorescence from the K(5^2D) to K(4^2P) transition upon excitation of the K(7^2S) state.[9] Given the known radiative lifetimes and the total deactivation cross sections for the K 7S and 5D states, the simulation shown in Fig. 6 yields the state-to-state rate coefficient 5.7×10^{10} cm^3 $molecule^{-1}$ s^{-1}, the only parameter included in the model. The model calculation is employed to fit the integrated fluorescence in the 7^2S-4^2P transition as the K(5^2D) state is excited by a two-photon process. Substitution of the coefficient obtained from Fig. 6 into the model yields a simulated profile which is in excellent agreement with the measurement of the integrated fluorescence from the 7^2S-4^2p transition (Fig. 7). Figs. 6 and 7 demonstrate the reliability of the determination for the 7S-5D transfer cross section. We conclude that the channel for energy depletion from the 7^2S state is predominantly physical quenching to the 5^2D state, although the KH product has been observed in the chemi-

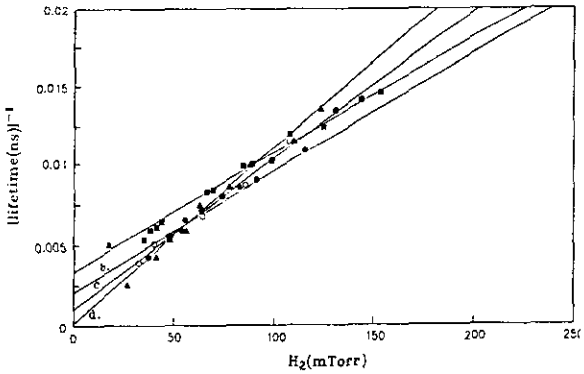

Fig. 4. Stern-Volmer plot of the reciprocal of effective lifetime for K n^2S (n = 8-11) states as a function of H_2 pressure. (a) n = 8 (■); (b) n = 9 (•); (c) n = 10 (o); (d) n = 11 (▲).

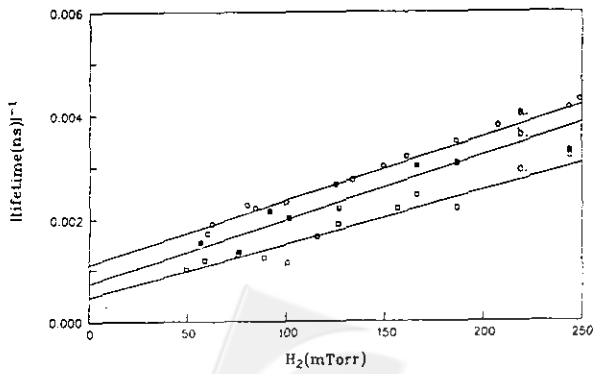

Fig. 5. Stern-Volmer plot of the reciprocal of effective lifetime for K n^2D (n = 6-8) states as a function of H_2 pressure. (a) n = 6; (b) n = 7; (c) n = 8.

cal reaction. The resulting state-specific cross section for 7S-5D is about 150 Å^2, and the reversed cross section for 5D-7S is about 23 Å^2. The latter corresponds to a branching ratio 60% of the total deactivation cross section measured in the 5^2D state. Thus the remaining channel of deactivation is expected to pass the lower energy states such as 6^2P.

ORBITAL ALIGNMENT ON SPIN-CHANGING COLLISION

We so far treated the sub-states of excited metal atom as if they are equally populated; therefore physical insight results from the averaged contribution of individual sub-state. Each sub-state of a metallic atom and its collision partner correlate symmetrically with a different molecular symmetry, that affects variably a reaction. The course of such orbital alignment of an electronically excited metallic atom on the cross sections of chemical reaction or energy transfer has drawn much attention of experimentalists[22-24] and theoreticians[25-27] during the past decade. Investigations have provided insight into the effect of the repulsive and attractive characters of a collision trajectory on near-resonant energy transfer,[23,25-27] an electron-transfer reaction,[28] a charge-exchange process,[29] an associative ionization reaction,[30] a quenching process,[24] or a fine-structure mixing collision.[31]

A crossed-beam apparatus has been generally employed to study atomic orbital alignment. For instance, the alignment dependence of energy transfer in the Ca-rare gas spin-changing collision has been carried out by Leone and his co-workers using a crossed-beam configuration,[23,32] consisting of an effusive beam for the metallic atoms and a supersonic jet for the collision partner. The Ca 5^1P_1 state was prepared by a linearly polarized laser; the fluorescence intensity of the Ca $5^3P_J \rightarrow 3^3D_J$ transition at 617 nm was then monitored as the angle Θ of the incident electric field vector with respect to the relative velocity vector was varied. They demonstrated that the measured fluorescence intensity I follows a cos 2Θ dependence, and the signal appears to be the maximum when the p-orbital is aligned perpendicular to the relative velocity vector, and to be the minimum when aligned parallel. The maximum intensity I_{max} or the minimum intensity I_{min} are related to the cross section of a near-resonant energy transfer when the asymptotic Π or Σ molecular state are locked and followed, respectively. Accordingly, the corresponding polarization is defined as $P = (I_{max} - I_{min})/(I_{max} + I_{min})$. For the case of Ca-Ar, the polarization gives a value of $(21 \pm 7)\%$.[32]

The second method is the far-wing scattering technique, with which Kleiber and co-workers have studied the orbital alignment dependence of the Ca($5^1P_1 \rightarrow 5^3P_J$) energy transfer by collision with He.[33,34] In the experiment a laser is tuned into the collision-broadened wings of the Ca $4^1S_0 \rightarrow 5^1P_1$ transition, exciting the CaHe quasimolecule at long range. The absorption in the far red wing is expected to excite predominantly the attractive Π state of CaHe, whereas the absorption in the far blue wing corresponds to excitation of the repulsive Σ state.[33,34] The observed cross-

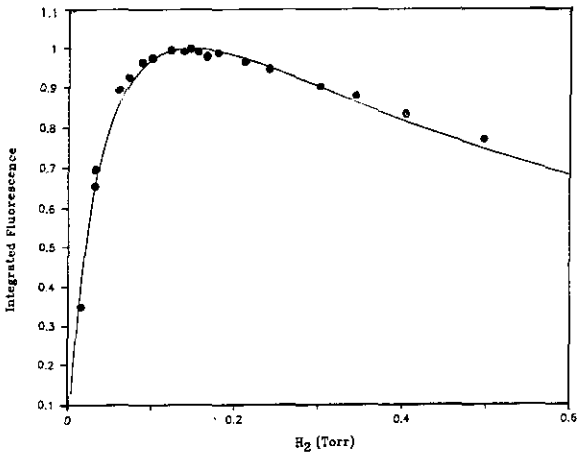

Fig. 6. Dependence on H_2 pressure of the integrated fluorescence monitored at the transition 5^2D-$4^2P_{3/2}$ following excitation of K to the 7^2S state. Solid circles indicate experimental data; the solid line indicates model calculation.

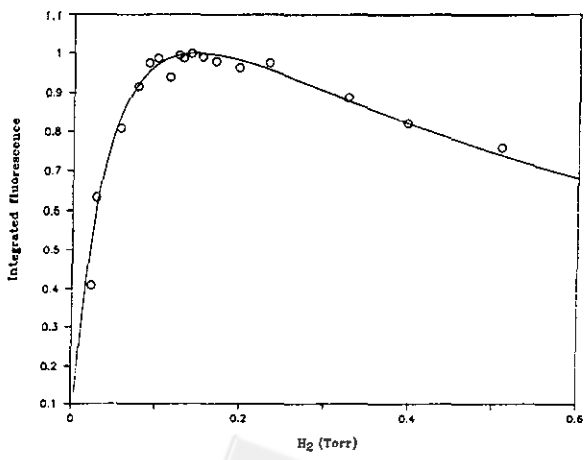

Fig. 7. Dependence on H_2 pressure of the integrated fluorescence monitored at the transition 7^2S-$4^2P_{1/2}$ following excitation of K to the 5^2D state. Solid circles indicate experimental data; the solid line indicates model calculation.

section dependence of the red/blue wing detunings are characterized according to a spin-orbit curve crossing model. Conceptually, if the long-range nonadiabatic Π-Σ electronic mixing is negligible, then the alignment effects obtained by the far-wing scattering technique are comparable with that by the crossed-beam methods. However, It has been found that the Σ and Π symmetry possibly scramble when the colliders approach each other,[23,26] so that the orbital initially aligned in the crossed-beam cannot be preserved completely in the collision. Kleiber et al. pointed out that the extent of orbital scrambling is reduced when the orbital alignment is prepared at a shorter internuclear distance. The alignment effect would reach almost 100% as a result of $\geq 70\ cm^{-1}$ detuning from the atomic transition.[34] However, this technique suffers from an extremely weak scattering signal for further detuning. In addition, the Π or Σ molecular states are presumed to represent an entirely attractive or a repulsive curve, respectively. The detunings may otherwise lead to a confusion of orbital interference.

The third method to measure the orbital alignment is by a half-collision of a van der Waals complex formed between the metal and the rare gas.[35] The Σ (or Π) molecular state of the complex is excited selectively as a result of blue shift (or red shift) near the atomic transition. By observing the "action spectra" of dissociated metallic atom with a probe laser fixed at a particular atomic transition, insight into the alignment effect on the chemical reaction or energy transfer is gained. Soep, Breckenridge and co-workers have successfully conducted the half-collision studies for CdXe,[36] ZnXe[37] and HgR[38] (R = rare gas or small molecules) van der Waals complexes.

Alternatively to the above techniques, we investigated the alignment effect with a single supersonic jet.[39] In order to compare with the crossed-beam measurement, we select the spin-changing collision in the Ca-Ar($4s5p\ ^1P_1 - 4s5p\ ^3P_J$) system as an example. In our apparatus the Ca metal is seeded in a supersonic free jet, for which Ar gas behind the nozzle behaves as both the collision partner and the carrier gas for free expansion. A laser with linearly polarized beam was used as excitation source. With a double Fresnel rhomb rotator, the electric-field vector of the impinging beam was rotated with respect to the direction of the molecular beam. Like the crossed-beam configuration, perpendicular alignment corresponds to excitation to the asymptotic Π molecular state, whereas parallel alignment results in excitation of the asymptotic Σ state. The experiment was done under conditions that an atom entrained in the beam encountered only a single collision in the interaction region during the period of fluorescence observation.

The collision-induced Ca atomic fluorescence signal of the $5^3P_J \rightarrow 3^3D_J$ transition at 617 nm as a function of the angle of electric field vector with respect to the jet beam direction is shown in Fig. 8. The fluorescence intensity varied as the orientation of the polarized radiation changed, and appeared the largest as the electric field vector is in a perpendicular alignment, but the smallest in a parallel alignment. The alignment effect (or polarization) diminished as the background Ar pressure increased. The decay dependence is closely related to both the quenching rate of Ca $5^1P \rightarrow 5^3P$ transition and the depolarization effect. The polarization, indicative of the orbital alignment effect on spin-changing collision for Ca-Ar system at 55 mTorr, is estimated to be (19 ± 1.5)%. The result is found consistent with the value of (21 ± 7)% obtained by Leone and co-workers using the crossed-beam apparatus.[32] A larger value would be expected if extrapolation were extended to zero pressure, at which polarization is considered free of interference from quenching or the depolarization processes. The latter occurred when the spatial orientation of angular momentum of the system changed during the collision. The polarization of Ca-H_2 reached 12% under 66 mTorr, consistent with the value of (13 ± 1)% reported previously.[40] A preliminary result on the Mg + H_2 reaction, carried out using a similar device, shows that the rotational quantum state distribution of MgH product depends upon the orientation of the polarized radiation. The facts described above demonstrate that one can conduct orbital alignment on both collisional energy transfer and chemical reaction processes with a supersonic jet.

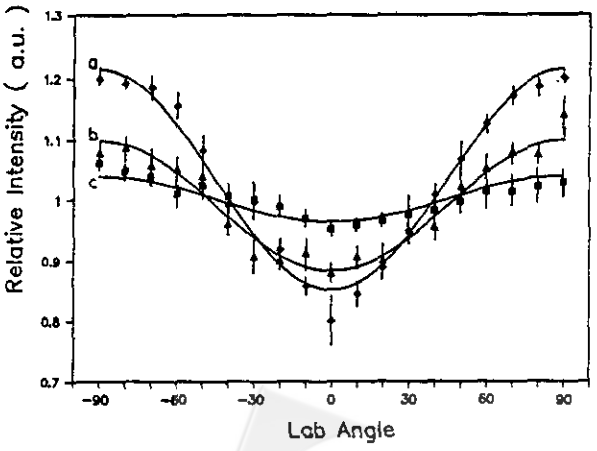

Fig. 8. Fluorescence intensity of the $5^3P_J \rightarrow 5^3D_J$ transition as a function of laser polarization orientation at various chamber background pressures of Ar: (a) 68 mTorr, (b) 280 mTorr, (c) 1.4 Torr.

Analogous to our apparatus, an Na effusive oven has been employed for the associative ionization reaction of $Na(3^2P_{3/2}) + Na(3^2P_{3/2}) \rightarrow Na_2^+ + e$.[30] The excited Na atoms collide because there is a distribution of speeds within the atomic beam. The relative velocity appears to be parallel to the beam. Although the design of the single-beam configuration is similar, the beam characteristics between the effusive oven and the supersonic jet differ markedly. First of all, the density of an effusive beam is small due to the restriction of the mean free path requirement, and then decreases as the square of the distance from the source.[41] Under the assumption of an isentropic, ideal gas expansion, the density in a supersonic jet is expected to be several orders of magnitude larger than that in an effusive beam, then decreasing as the $2/\gamma$ power of the distance downstream from the orifice;[41,42] γ indicates the heat capacity ratio C_p/C_v. The velocity of the effusive beam is governed by the Maxwell-Boltzmann distribution and characterized by the reservoir temperature. The collisions occur as the rapid particles in the stream overtake the slow ones. In contrast, the jet beam velocity reaches its terminal value quickly in the early expansion and cannot be further increased, independently of the reservoir pressure or the distance downstream.[42] Increase of the distance downstream or the reservoir pressure may lead to a colder beam, thereby narrowing the spread distribution of the terminal mean velocity. The terminal mean velocity of a monatomic ideal gas corresponds to a factor of $(5/3)^{1/2}$ times as large as the root-mean-square velocity in an effusive beam.[43] The collision frequency per molecule occurring in an effusive beam, with density n, collision cross section σ and mean velocity ν of molecules in the source, is estimated to be $(2)^{1/2}n\sigma\nu(7\text{-}4(2)^{1/2})/4$, explicitly independent of the temperature.[41] The collision frequency of molecules in a supersonic jet with mean velocity ν_0 and temperature T_0 in the reservoir is determined according to the formula of $(2)^{1/2}n\sigma\nu_0(T/T_0)^{1/2}$, depending upon the square root of the beam temperature T. This factor offsets the effect of the density, so that the molecules entrained in the jet beam are considered free of collisions under appropriate conditions. Finally, the translational temperature of molecules in the jet can be effectively governed depending upon the ratio of X/D (X: distance downstream from the nozzle orifice; D: nozzle diameter.) and the reservoir pressure. Hence the measurement of temperature (or kinetic energy) dependence of orbital alignment effect becomes accessible using the device of a supersonic jet, although it is beyond the scope of this work.

We compare the current method to the crossed-beam configuration in the following.

1. The direction of the relative velocity vector in the single supersonic jet is invariably along the molecular flow direction of the free jet, independent of the colliding species. The seeded Ca velocity is parallel to the carrier gas Ar velocity. The collision here is considered to be mainly along one dimension. In contrast, in the crossed-beam apparatus, the direction of the relative velocity vector varies depending upon the masses of the collision partners and their individual velocities.[23,32] The collision occurs in a two-dimension plane, thus the relative velocity is spread over this plane. As a result, the orientation of polarized radiation in a different system must be adjusted to some extent to lock and follow into a specific molecular state.

2. With the crossed-beam apparatus, the alignment effect is measured under a single collision condition. In our work, by appropriately selection of the operating conditions for the supersonic jet and the interaction region, the measured polarization can also be resulted from a single collision event. For example, given a pressure 1 atm behind the nozzle, 10 $Å^2$ collision cross section, mean velocity of 6×10^4 cm s^{-1} at a nozzle temperature 800 K, and the interaction region X/D = 7, then the collision rate is estimated to be 6×10^5 s^{-1}. This value indicates that a secondary collision in the interaction region may well be negligible during the 10-100 ns period for the $Ca(5^3P_J\text{–}3^3D_J)$ fluorescence observation. The argument is still valid even though the collision cross section is enlarged 10 times. Under the condition of a small background pressure (or extension to zero pressure), the resulting polarizations are found consistent with those from the crossed-beam experiments. The polarization becomes gradually depleted as the background pressure increases because of the interference by the quenching process and the depolarization effect. This enables us to extract information on the roles of the competing processes. In addition, by varying the X/D ratio and the reservoir pressure, it becomes possible to study the temperature dependence of the orbital alignment effect on energy transfer or chemical reaction.

3. Optical alignment in our work is much easier than in a crossed-beam experiment, as only two-beam interaction is involved instead of a three-beam alignment. In addition, in the crossed-beam configuration which employs a Ca effusive beam, a smaller density at the interaction region is expected than that generated by a supersonic jet. For instance, the Ca vapor at the nozzle temperature 800 K having a reservoir density 1.5×10^{13} atoms cm^{-3} can produce a number density 0.7×10^{10} atoms cm^{-3} in the interaction region in the crossed-beam experiment reported by Leone and co-workers.[32] In our case, we expect the Ca density interacted to be 4.7×10^{10} atoms cm^{-3}, having about 6 times en-

hancement, under the same nozzle temperature. Comparing the alignment result shown in Fig. 8 with that reported previously for the case of Ca-Ar,[32] we believe that a better signal-to-noise ratio obtained in this work is mainly attributed to this factor.

4. The molecules in a supersonic jet are expected to be translationally colder, thereby leading to a much narrower spread of the Ca velocity distribution. In this manner, orbital scrambling is reduced, compared to the use of a Ca effusive beam in the crossed-beam apparatus. One can form a van der Waals complex such as CaAr under the conditions of low temperature. If a laser is tuned into the CaAr molecular transition, the Π or Σ molecular states can be selectively excited. In such a case, the alignment is prepared at a shorter internuclear distance and orbital scrambling should be minimized. This effect has already been demonstrated in the far wing scattering experiment.[33,34]

REACTION MECHANISM: INSERTION VS. ABSTRACTION

In a reaction mechanism of a three-particle system we choose $Mg^* + H_2$ as the example. For this reaction, Breckenridge et al. used a pump-and-probe method to demonstrate that the rotational energy of the MgH product was characterized by a bimodal distribution.[44] The large component over the higher rotational quantum states was intuitively considered previously to follow a mechanism of Mg insertion into the H_2 bond by a side-on attack, thus leading to a triangular intermediate MgH_2. As one terminal H atom escapes, a torque is exerted upon the remaining MgH. For this reason much energy is converted into the form of rotation. In contrast, a small portion of lower rotational energy distribution was subject to a reactive approach having a collinear configuration. Thus the mechanism of H abstraction by the end-on attack may not affect the rotational energy of MgH significantly. Kleiber et al. measured the yield of MgH product in the far wing absorption of the MgH_2 collision complex as a function of detuning from the $Mg(^1P-^1S)$ resonance transition.[45,46] The branching ratio of the lower rotational [MgH(v" = 0, K" = 6)] to the higher rotational [MgH(v" = 0, K" = 23)] reaction product displayed a slight difference from the theoretical prediction of no dependence on the entrance-channel control model. Accordingly they suggested that the nascent product of the subject reaction may correlate with the entrance-channel geometry. A further investigation by Breckenridge et al. using isotopic hydrogen as reactants, however, showed a profile coincidence between the MgH and the MgD rotational population distributions.[47] The study of the isotopic effect on the bimodality indicates that the reaction is due solely to Mg insertion. The existence of ambiguous causes of bimodality prompted us to carry out this reaction.[48,49] We investigated the temperature dependence of the nascent rotational energy distribution of MgH produced by the reaction of $Mg(^1P_1)$ with H_2, in an attempt to clarify the mechanism leading to the bimodal distribution observed for MgH. Because the potential barriers differ between the collinear and the bent collisional conformations, these two reactive mechanisms are expected to respond differently to the effect of temperature. Thereby determination of the predominant mechanism becomes feasible.

By means of the pump-and-probe technique, the laser-induced fluorescence (LIF) of MgH product was measured in a heat-pipe oven. Fig. 9 shows a portion of the LIF spectrum of MgH ($A^2\Pi - X^2\Sigma^+$) in the range 518-522 nm in the reaction of $Mg(^1P_1)$ with H_2 gas at 5 Torr. Because of limited laser resolution we avoided the region of complicated overlapping with the R and Q branches and thus concentrated on the P_1 and P_2 branches of the (0,0) band. Even so, the bandhead nature makes a complete resolution of this branch difficult, and a computer simulation to deconvolute each line from P(10) to P(21) is necessary. The resolved peak of the P branch was converted into a plot of the rotational population distribution against the rotational quantum states K (Fig. 10). The distribution is bimodal in agreement with that observed by Breckenridge et al.[44] The distribution is in the nascent manner, because the delay between pump and probe laser pulses is about 5-8 ns, so brief that rotational relaxation by gaseous H_2 is negli-

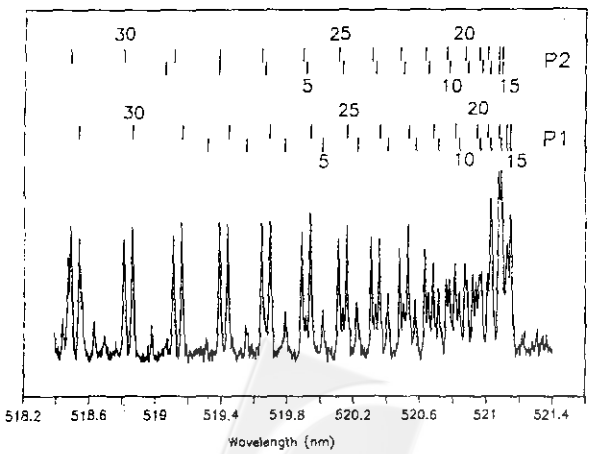

Fig. 9. Part of the LIF spectrum for the MgH(0,0) band of the $A^2\Pi - X^2\Sigma^+$ transition.

gible.

Presumably the bimodal nature of the MgH product of the reaction of $Mg(^1P_1)$ with H_2 is ascribed simultaneously to both end-on and side-on attacks. As H_2 is replaced with HD, the isotopic branching ratio of H/D may be expected to produce a value > 1 for the large component of the high rotational state distribution, but a value < 1 for the small rotational state distribution.[50,51] Breckenridge and co-workers found that the ratio of MgD/MgH gave a value, 0.9 ± 0.12, and the normalized profile of the MgH bimodal distribution coincided with that of MgD product.[47] The lack of a significant isotopic effect indicates that the bimodality originated from a single mechanism, because the otherwise opposite tendency of influence of the isotopic effect would enlarge the difference between the MgH and MgD rotational state distributions. Accordingly they concluded that the insertive mechanism is the only one.

Thus far, there have been three methods usually employed to treat the collision mechanism of the atom-diatom reaction. The spectral method characterized the rotational quantum-state distribution of the nascent product; thereby some indication of the geometry of approach in a reaction is deduced. Alternative means to identify the collisional orientation of a three-particle system include crossed beams and the isotopic effect; in the former, backward scattering in the center-of-mass coordinate is taken to denote an end-on approach, whereas the symmetric scattering patterns are found in a side-on approach, by which the intermediate formed following an attractive surface may persist longer.[52] In contrast, an isotopic branching ratio of H/D, for a reaction of A + HD $\longrightarrow$ AH (or AD) + D (or H), provides a qualitative indication of occurrence of either abstraction or insertion. When the reactions are dominated by insertion, the ratios of H/D are expected to be > 1, whereas abstractive reactions are expected to lead to ratios < 1.[50,51] In fact, the observed variation of the ratios is mainly limited to the range 0.5-2. Such an insignificant effect might be easily buried in a small signal-to-noise ratio.

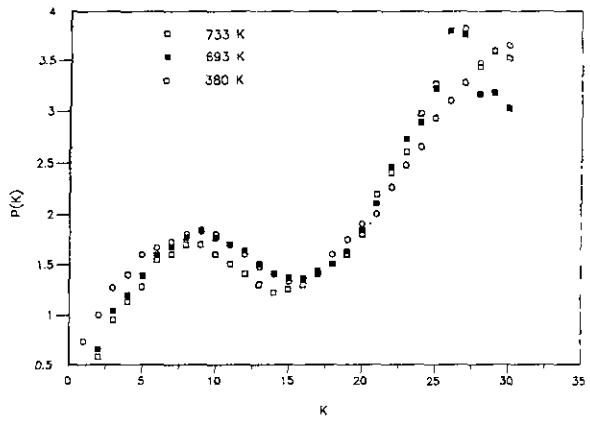

Fig. 10. Comparison of normalized, bimodal population distribution for the nascent product MgH at various temperatures. (■) and (□) denote our results at 693 and 733 K, respectively; (o) denotes the result at 380 K from Breckenridge and co-workers.

We consider the causes of bimodality from an alternative aspect. Considering a collinear ($C_{\infty v}$) and a bent (C_{2v}) collisional conformation between $Mg(^1P_1)$ and H_2, respectively, Chaquin et al.[53] calculated the dynamical potential energy surfaces, and predicted the reactive pathways corresponding to end-on or side-on approaches. As the insertive reaction occurs with a bent MgH_2 intermediate, the reaction coordinate leading to MgH product tracks an attractive $^1B_2$ surface without suffering from an activation barrier. In contrast, for a collinear approach of $Mg(^1P_1)$ toward H_2, there exists a barrier as large as 1.8 or 1.7 eV as either a $^1\Sigma^+$ or a $^1\Pi$ surface is followed, respectively. As the barrier differs for MgH produced between collinear and bent colliding geometries, these two reaction mechanisms may respond differently to the temperature effect. In our experiments, the distribution of rotational population of the nascent MgH product obtained at 733 K was normalized and compared with that at 693 K, and with the results at 380 K by Breckenridge and co-workers. As shown in Fig. 10, the bimodal profiles coincide satisfactorily within experimental error.

In agreement with the conclusion drawn from the isotopic effect, the results of the temperature dependence demonstrate that the bimodality originates from a single reaction mechanism, in which $Mg(^1P_1)$ approaches H_2 from the side to attack along the attractive $^1B_2$ coordinate. As the end H atom escapes from the bent intermediate, a torque acts on the remaining MgH product, thereby leading to a high rotational population distribution. If the MgH is produced by an end-on attack, a barrier estimated as large as 1.7 eV has to be overcome. Experimentally a linear Mg-centered MgH_2 product has been observed at 12 K.[54] For these reasons, it seems impossible to have the abstractive reaction occurring simultaneously.

What is the influence of temperature on bimodality, if the distributions at different extents of rotational excitation stem from different mechanisms, i.e., abstraction and insertion occur simultaneously. If a reaction coordinate follows the repulsive potential surface in the entrance channel geometry, then the rate of formation of the product is expected to increase with increasing temperature, according

to the Arrhenius theory. The reaction rate decreases with increasing temperature if the reaction proceeds without an energy threshold; the prediction of temperature effect based on a model of a transient complex,[55] which has been successfully employed to interpret an unusually large quenching cross section, is consistent with this absence of an energy threshold. The intermediate complex formed by the substrate and the quencher is dominated by the attractive long-range interaction in the entrance coordinate. With increased temperature, the lifetime of the complex decreases such that the energy originally deposited in the substrate cannot be significantly transferred to all possible exit channels. The resulting quenching rate appears to decrease as temperature increases. Accordingly, the temperature dependences of the abstractive and insertive reactions show opposite influence upon the different regions of the rotational distributions, respectively, of the MgH product. The lack of effect of temerature in the range 380-733 K on the MgH rotational population distribution confirms that the reaction is initiated only by insertion. Because the temperature is variable continuously, unlike the isotopic effect, the temperature dependence is expected to magnify the difference between the profiles of the rotational distributions more significantly, if both insertion and abstraction have contributions.

PHOTODISSOCIATION

Photodissociation of diatomic molecules is extensively employed to generate hot fragments, with which investigation of the dependence of a chemical reaction on kinetic energy can be carried out. To control sufficiently the energy carried in a reaction, it is crucial to understand thoroughly the quantum yields of the fragments concerned. To determine the quantum yields of the photofragments in different electronic states, the relative intensity measurement of emission as a result of an individual excited fragment is inefficient. For instance, in the 193 nm photodissociation of KI, K atoms are expected to be fragmented into various states. For those excited states with long lifetimes, the fluorescence signal may be obscured by the effect of population redistribution. Analogously, in the measurement of the quantum yield of the excited $I(5^2P_{1/2})$ atom by means of fluorescence detection, collisional deactivation can interfere with the observation of ir emission having a radiative lifetime as long as 0.13 s.

To produce a more accurate quantity for the yields of photofragments than that obtained by the fluorescence method, we employed a resonance multiphoton ionization (REMPI) technique to monitor the fragmented I atoms following photodissociation of KI at 193 nm.[56] The iodine ions associated with the $I(5^2P_{3/2})$ (or $I(5^2P_{1/2})$) state were detected by the (2 + 1) REMPI scheme through the $^2D_{5/2}$ (or $^2D_{3/2}$) intermediate states. Thereby the populations of the nascent I fragment in its fine-structure components was determined; information about the nascent K atoms state distribution was also inferred.

The radiation sources of the REMPI apparatus comprised one ArF excimer laser for photolysis of the KI sample, and the other excimer laser-pumped dye laser, tunable in the range 588-644 nm with Rhodamine B dye, to monitor the fragmented I atoms. The sample KI was deposited in a five-armed heat-pipe oven, operated at 673 ± 2 K; thus the vapor pressure corresponded to 0.8 mTorr. As shown in Fig. 11, the results of iodine ions, associated with the population in the ground and its spin-orbit excited states, are obtained using the (2 + 1) REMPI technique through $^2D_{5/2}$ and $^2D_{3/2}$ as intermediate states respectively. Because the iodine fine-structure components are the only exit channels following photodissociation, the quantum yield of $I(5^2P_{3/2})$ is defined as $S(P_{3/2})/[S(P_{3/2}) + S(P_{1/2})]$. Here $S(P_{3/2})$ and $S(P_{1/2})$ indicate the population of nascent I fragment in its two fine-structure states. The following equation was used to relate the ion signals to the relevant state populations:

$$\frac{\mathrm{Ion}(P_{1/2})}{\mathrm{Ion}(P_{3/2})} = k\frac{S(P_{1/2})}{S(P_{3/2})} \qquad (2)$$

Using an excitation scheme identical to ours, Bersohn and co-workers detected the laser-induced vuv fluorescence from the excited I atoms in the experiment of CH_3I photodissociation,[57] and derived a calibration factor k =

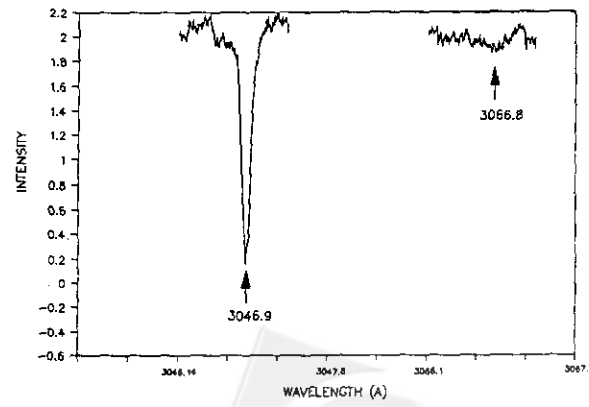

Fig. 11. The three-photon (2 + 1) REMPI signals of $I(5^2P_{3/2})$ and $I(5^2P_{1/2})$ atoms obtained following the scheme described in the text.

1.12 for such an iodine probing scheme. We adopted the same calibration factor used in Eq. 2, assuming that the I atoms excited to both $^2D_{5/2}$ and $^2D_{3/2}$ states have the same ionization cross section. We obtained the quantum yield of $I(5^2P_{3/2})$ resulting from the KI photodissociation at 193 nm as (97 ± 3)%. In photodissociation of alkyl iodide, the electron-withdrawing groups favor I in the spin-orbit excited state, whereas the electron-donating groups favor I in its ground state.[57,58] In our work the K atom as an electron-donating partner follows the same trend.

The $5^2P_J \rightarrow 4^2S_{1/2}$ and $4^2P_J \rightarrow 4^2S_{1/2}$ transitions are the only two emission lines observed with a monochromator scanned over the region 300-900 nm following 193 nm photodissociation of KI. Provided that $K(4^2P_J)$ and $K(4^2S_{1/2})$ are also fragmented, the iodine atom populated to its spin-orbit excited state becomes energetically accessible. K atoms in the 4^2P_J state for instance have excess energy ~ 12000 cm^{-1} enough to compensate for the energy defect between the $I(5^2P_J)$ doublets about 7603 cm^{-1}. The excess energy carried by these lower states is unlikely to be totally transfered into the translational energy, but not partly into the internal energy of the iodine atoms. In photodissociation of NaI with a femtosecond laser, the very early stage of cleavage shows that the NaI molecule is bounced back and forth in a quasi-potential well, adiabatically formed from an excited repulsive covalent potential curve and an ionic potential curve.[59] The result leads to a leak about 10% yield of the Na atom each period. Obviously, NaI in photodissociation is exposed simultaneously to repulsive and attractive forces, and consequently retarded from breaking apart. Having a character similar-to NaI, KI upon photodissociation seems hard to fit in the impulsive model.[60] Based on this model, the KI sample is expected to break apart abruptly upon laser irradiation, as if a repulsive force is exerted upon it; thereby the excess energy carried by the fragments is otherwise converted completely into translational energy.[60] Accordingly, the observed extremely large quantum yield for the $I(5^2P_{3/2})$ state indicates that the dissociation channels into lower states, especially 4^2P_J and $4^2S_{1/2}$ are negligible. Wiesenfeld and co-workers, who measured the time-resolved fluorescence of an individual excited K fragment in the 193 nm photodissociation of KI, found that more than 80% K is scattered into the 5^2P_J state, but insignificantly contributed to the 3D and 5S states within their detection conditions.[61] This result was verified in an experiment on the pressure dependence of the $4^2P_J \rightarrow 4^2S_{1/2}$ fluorescence detection;[62] based on an assumption that the initial fragments in the 3D and 5S states are zero, the theoretical prediction agrees with the experimental results.[62] Therefore, we conclude that the potassium atoms are predominantly partitioned to the 5^2P_J state.

What is the branching ratio of the predominant photofragment of K 5^2P_J fine-structure components? We have developed an efficient method using a three-level kinetic model to refine the branching ratio determination of the K $5^2P_{3/2}$ and $5^2P_{1/2}$ fine-structure states following 193 nm photodissociation of KI in the presence of foreign gases.[63,64] Through the rate equations of the model we need one parameter to fit the measurement of branching ratio as a function of pressure of foreign gas to derive its zero-pressure value. As this model takes into account the collision-induced energy transfer between the 5^2P_J doublets, the determined values appear to be more accurate than measurements of fluorescence intensity ratio under the low-pressure condition. We further examine the reliability of the kinetic model. The branching ratio of the nascent photofragment is expected to be independent of the presence of foreign gases. Accordingly, although the collision-induced mixing rate between the fine structure components may differ for different foreign gases, the determined nascent branching ratio should be identical. The quenching rate coefficients of the 5^2P_J doublets and the mixing rate coefficients between them induced by the collision partners of Ar, He, H_2, CH_4, and CO_2 were measured. Given these rate coefficients, the nascent branching ratio was deduced.

A three-level system, consisting of the spin-orbit states of interest, $5^2P_{1/2}$ and $5^2P_{3/2}$, and other states which form all possible channels of the population depletion, was employed to interpret the kinetic mechanism of the photofragments. The processes are

$$KI + h\nu(193\ nm) \longrightarrow K(5^2P_J) + I(5^2P_{3/2}) \quad (3)$$

$$K(5^2P_{3/2}) + M \underset{k_{-1}}{\overset{k_1}{\rightleftharpoons}} K(5^2P_{1/2}) + M \quad (4)$$

$$K(5^2P_{3/2}) \xrightarrow{k_2} K(4S, 3D, 5S) + h\nu' \quad (5)$$

$$K(5^2P_{3/2}) + M \xrightarrow{k_3} K(4S, 4P, 3D, 5S) + M \quad (6)$$

$$K(5^2P_{1/2}) \xrightarrow{k_4} K(4S, 3D, 5S) + h\nu'' \quad (7)$$

$$K(5^2P_{1/2}) + M \xrightarrow{k_5} K(4S, 4P, 3D, 5S) + M \quad (8)$$

Here M indicates the foreign gases. Time evolution of the population density of the $K(5^2P_{3/2})$ and $K(5^2P_{1/2})$ states is easily solved from the coupled rate equations related to the schemes described above.[63] If the nascent branching ratio

of the K $5^2P_{3/2}$ component is defined as $x = A_0/(A_0 + C_0)$, in which A_0 and C_0 are the initial population density of $K(5^2P_{3/2})$ and $K(5^2P_{1/2})$ respectively, the intensity ratio F_2/F_1 is expressed as a function of this branching ratio,

$$\frac{F_2}{F_1} = \frac{x(k_3[M] + k_4) + k_{-1}[M]}{(k_1 + k_5)[M] + k_2 - x(k_5[M] + k_2)} \quad (9)$$

where F_1 and F_2 are the fluorescence intensity, integrated over the entire temporal profile monitored experimentally for the transition $5^2P_{1/2} \rightarrow 4^2S_{1/2}$ and $5^2P_{3/2} \rightarrow 4^2S_{1/2}$, respectively. Given the rate coefficients k_i, i = 1 – 5 and -1, the partitioning of nascent photofragment K in the $5^2P_{3/2}$ and $5^2P_{1/2}$ states is derived by fitting the parameter x to the measurement of the dependence on foreign gas pressure of the intensity ratio F_2/F_1.

These rate coefficients, k_2, k_3, k_4 and k_5, were determined by measuring time-resolved fluorescence from the $5^2P_J \rightarrow 4^2S_{1/2}$ transition as a function of the foreign gas pressure following photodissociation of KI at 193 nm, and then applying the Stern-Volmer equation. The results (Table 3) agree with those reported previously. To measure energy transfer between the $K(5^2P_J)$ doublets, the KI sample was replaced with potassium metal in the heat-pipe oven operated at 100 ± 1 °C and the light source was changed to an excimer laser-pumped dye laser emitting at 404 nm. The mixing rate coefficients k_1 and k_{-1} were deduced from the detection of both resonance and sensitized fluorescences. The intensity ratio R_1 of the sensitized-to-resonance fluorescence upon excitation of $K(5^2P_{1/2})$ is[63,65,66]

$$R_1 = \frac{A_{3/2}\, k_{-1}[M]}{A_{1/2}[(k_1 + k_5)[M] + k_2]} \quad (10)$$

When another fine-structure state $K(5^2P_{3/2})$ was excited, analogously, the intensity ratio R_2 of sensitized-to-resonance fluorescence is

$$R_2 = \frac{A_{1/2}\, k_1[M]}{A_{3/2}[(k_{-1} + k_3)[M] + k_4]} \quad (11)$$

where $A_{3/2}$ and $A_{1/2}$ are the Einstein coefficients for spontaneous emission in the transitions $5^2P_{3/2} \rightarrow 4^2S_{1/2}$ and $5^2P_{1/2} \rightarrow 4^2S_{1/2}$. In this model, k_1 and k_{-1} are determined independently without involving the principle of detailed balance.

As shown in Fig. 12, measurements of dependence on the foreign gas pressure for the first-order rate coefficients Z_{12} and Z_{21}, which equal $k_{-1}[M]$ and $k_1[M]$, yield separately the cross sections of energy transfer for each quencher. The results (Table 4) show that the capability of the foreign gases to cause the energy transfer between the 5^2P_J doublets follows the trend $H_2 \sim Ar < He \sim CH_4 < CO_2$.

Table 3. The Calculated Fine-Structure Mixing Rate Coefficients (k_1 and k_{-1} in Units of cm^3/mol s). The Determined Radiative Rate Coefficients (k_2 and k_4 in Units of s^{-1}) and Quenching Rate Coefficients (k_3 and k_5 in Units of cm^3/mol s) for the $5^2P_{1/2}$ and $5^2P_{3/2}$ Doublets by Collisions with Five Foreign Gases

Gas	$k_1(10^{-9})$	$k_{-1}(10^{-9})$	$k_2 = k_4(10^6)$	$k_3 = k_5(10^{-10})$
Ar	0.82	1.51	7.29	1.7
He	2.07	4.25	7.27	4.7
H_2	2.03	3.72	7.27	2.89
CH_4	1.30	2.35	7.19	7.3
CO_2	3.00	6.19	7.24	8.2

A polyatomic molecule is expected to have a larger efficiency than a noble gas, because its internal states provide more channels for energy transfer in the collision. Herm and co-workers reported that the outer valence electron configuration of a quencher is closely related to its quenching efficiency.[67] They found that a quencher whose lowest unoccupied molecular orbital (LUMO) is strongly an-

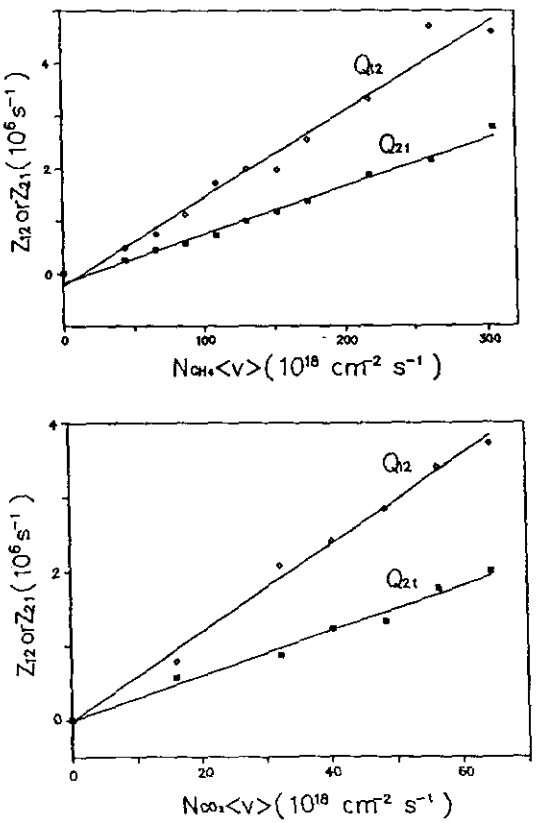

Fig. 12. Measurement for CH_4 and CO_2 pressure dependence of the first-order rate coefficients Z_{12} and Z_{21} of fine-structure energy transfer. The average relative velocity <v> is 834 m s^{-1} for K^*-CH_4 collision and 618 m s^{-1} for K^*-CO_2 collision under the Maxwellian-Boltzmann distribution at 100 ± 1 °C.

Table 4. Collision-Induced Mixing Cross Section of 5^2P_J Doublets. Q_{21} and Q_{12} Indicate the Respective Cross Section for the $5^2P_{3/2} \rightarrow 5^2P_{1/2}$ Transition and Its Reverse Process

Gas	Q_{12}(Å^2)	Q_{21}(Å^2)	Reference
Ar	149 ± 9	81 ± 7	(64)
	145 ± 5	79 ± 4	(63)
	317 ± 45	153 ± 22	(66)
	139 ± 3		(70)
He	208 ± 18	101 ± 6	(64)
	561 ± 84	260 ± 39	(66)
	156 ± 17		(70)
H_2	134 ± 6	72 ± 5	(63)
CH_4	190 ± 21	105 ± 8	(64)
CO_2	621 ± 41	301 ± 20	(64)

tibonding is less efficient than an unsaturated molecule; the latter is characterized by a quenching cross section comparable to or somewhat larger than "gas-kinetic" estimate. Accordingly CO_2 is expected to be more active than CH_4, thus leading to a larger cross section of energy transfer.

Although the polarizability of He is much smaller than that of Ar,[68] an abnormally large cross section of energy transfer caused by He was observed in our work and similar result was also reported by Krause's group.[65,66] Nikitin calculated the cross section for transition between the fine-structure components of alkali atoms by collision with the noble gas in a strong coupling approximation;[69] he concluded that the cross section of energy transfer increases almost exponentially with increasing relative velocity between the alkali atom and the noble gas, but quadratically proportional to the characteristic collision radius. Although the determination of characteristic collision radius relies upon a dedicated potential-energy curve obtained for the alkali-noble gas interaction, polarization interaction between the colliders contributes negligibly to electrostatic splitting.[69] While the characteristic collision radii of K-He and K-Ar are assumed similar, the relative velocity for K-He collision, being twice as large as that of the K-Ar collision, may be the main factor to cause a larger cross section of energy transfer.

The ratio Q_{12}/Q_{21} obtained in this model agrees with that predicted by the principle of detailed balance under the condition of thermal equilibrium. To learn the appropriate rate coefficient for the nonequilibrium condition of photodissociation, it is necessary to estimate the relative velocity distribution for the photofragments. The recoil velocity of K* in the center-of-mass frame is estimated to be 821 m s^{-1} for photodissociation at 193 nm, which is converted to a value of 848 m s^{-1} at 400 °C for the most probable speed V_T of K* in the laboratory frame.[63]

The bimolecular rate coefficient k_q is related to the quenching cross section S_q according to the expression

$$k_q = \int_0^\infty S_q(g)P(g)g\,dg \qquad (12)$$

where g is the relative speed between the K* atom and the target molecule; P(g) is the relative speed distribution for the K fragment and the quencher. We assume that the fragment K has a single laboratory velocity V_T at 400 °C, whereas the target molecules follow a Maxwellian velocity distribution. Accordingly, the corresponding rate coefficients k_i and k_{-1} under the condition of photodissociation were derived (Table 3).

Given these rate coefficients of k_i (i = 1-5 and -1), only one parameter in Eq. 9 needs to be adjusted to fit the pressure dependence of the branching ratio. Comparison of the measured value of the integrated fluorescence intensity ratio with the theoretical counterpart over the pressure range in Fig. 13 shows excellent agreement. The result leads to a respective branching ratio of 0.800, 0.798, 0.791, 0.797 and 0.785 for K($5^2P_{3/2}$) measured by collisions with

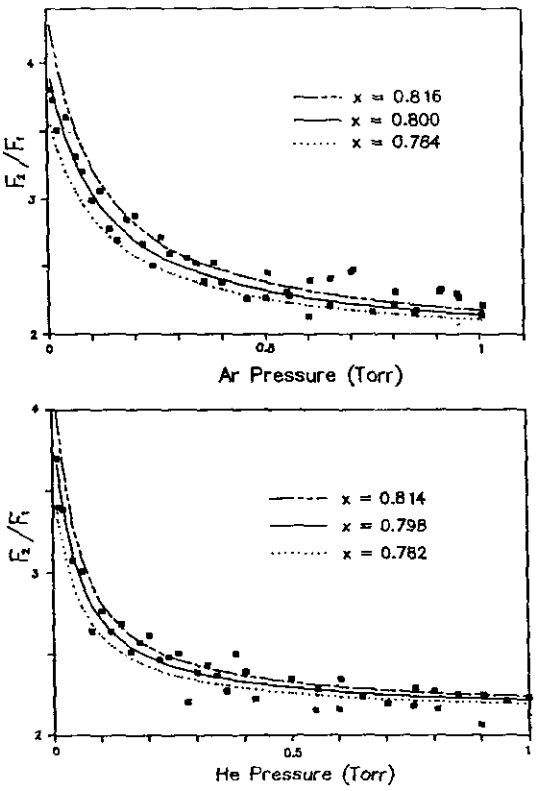

Fig. 13. Measurement of the fluorescence intensity ratio F_2/F_1 as a function of foreign gas pressure. x is the branching ratio of K($5^2P_{3/2}$). The solid line corresponds to the best-fit x value, 0.800 for Ar and 0.798 for He. Dashed line and dot-dashed line indicate the best-fitting curves when x differs by 2%.

Ar, He, H_2, CH_4 and CO_2, respectively. The fitting curve is sensitive to a change of the branching ratio. A 2% change produces a remarkable discrepancy from the experimental data (Fig. 13). Therefore, the accuracy of each branching ratio is estimated to be ± 1%. Although the foreign gases involved may result in various mixing rates for the doublets, the branching ratio deduced at the zero-pressure condition converged to 0.796 ± 0.004, an average value from those related to Ar, He, CH_4 and H_2 collisions. The result obtained with CO_2 collision appears slightly smaller and needs to be verified; therefore, we neglected its value in the average.

Finally, such a simulation was also used to examine the reliability of the mixing rate coefficient by collision with foreign gases. Our results of fine-structure mixing cross sections by Ar and He collision are consistent with the theoretical calculation, but both measurements appear to be smaller by half of those from the Krause's group.[65,66] When the parameters of mixing rate coefficients to fit the branching ratio are replaced by the values from Krause's group (Fig. 14), their values result in a remarkable discrepancy from the observed pressure dependence measurement of the branching ratio. Thus we believe that our mixing cross sections of fine-structure components by Ar or He collisions are more reliable. Although there is no literature value for comparison with our case of H_2 and CH_4 collisions, the quality of branching ratio fitting and the accuracy of the resulting value indicate that the cross sections obtained are also reliable. As to the CO_2 case, due to a rapid interaction of CO_2 with excited K, the pressure of CO_2 in the oven keeps decreasing; it is therefore difficult to maintain a constant pressure in a closed system while measuring the time-resolved fluorescence. The resultant branching ratio appears slightly smaller than those determined with Ar, He, CH_4 and H_2 collisions. According to our kinetic model, the mixing rate coefficients can also be derived inversely, provided that the branching ratio of the 5^2P_J doublets is given. In this manner, the Q_{12} and Q_{21} cross sections by CO_2 collision are estimated to be (408 ± 32) and (211 ± 18) $Å^2$ as a result from the branching ratio as the average value 0.796 ± 0.004 and the Q_{12}/Q_{21} ratio 1.89 based on the principle of detailed balance. The results deviate from our observed values, and suggest that the measurement by CO_2 collision needs to be confirmed.

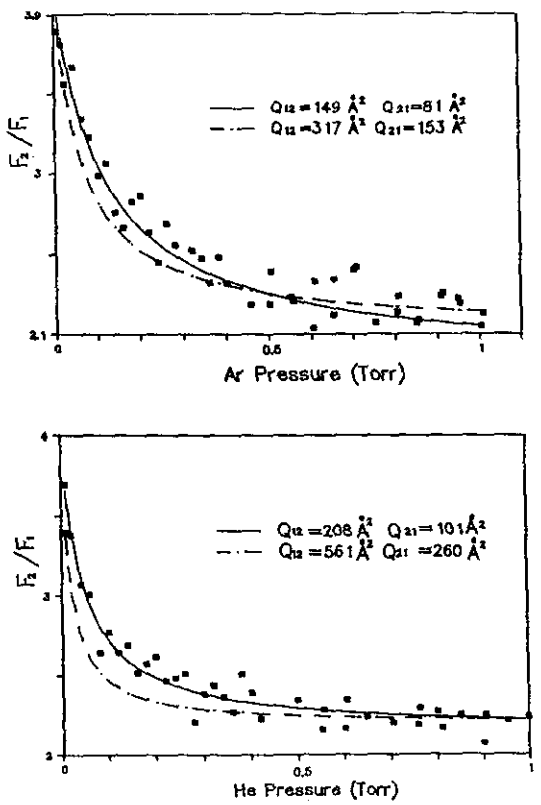

Fig. 14. Comparison of the best-fitting curves for various fine-structure mixing cross sections with the branching ratio of the $5^2P_{3/2}$ state fixed at 0.800 for Ar and 0.798 for He.

ACKNOWLEDGMENT

The author wishes to thank his co-workers for making this paper a reality and the National Science Council of the Republic of China for financial support.

Received August 28, 1992.

Key Words

Dynamics; Kinetics; Metal atoms; Orbital alignment; Photodissociation.

REFERENCES

1. Sayer, B.; Farray, M.; Lozingot, J.; Berlande, J. *J. Chem. Phys.* **1981**, *75*, 3894.
2. Visticot, J. P.; Farray, M.; Lozingot, J; Sayer, B. *J. Chem. Phys.* **1983**, *79*, 2839.
3. Crepin, C.; Picque, J. L.; Rahmat, G.; Verges, J.; Vetter, R.; Gadea, F. X.; Pelissier, M.; Spiegelmann, F.; Malrieu, J. P. *Chem. Phys. Lett.* **1984**, *110*, 395.
4. Rahmat, G.; Spiegelmann, F.; Verges, J.; Vetter, R. *Chem. Phys. Lett.* **1987**, *135*, 459.

5. Lin, K. C.; Chang, H. C. *J. Chem. Phys.* **1989**, *90*, 6151.
6. Schmidt, H.; Weiss, P. S.; Mestdagh, J. M.; Covinsky, M. H.; Lee, Y. T. *Chem. Phys. Lett.* **1985**, *118*, 539.
7. Reiland, W.; Jamieson, G.; Schulz, C.; Tittes, H.; Hertel, I. V. In *Electronic and Atomic Collision*; Eichler, J; Hertel, I. V.; Stolterfoht, N., Eds.; Elsevier: Amsterdam, **1984**; p 693.
8. Rossi, F.; Pascale, J. *Phys. Rev. A* **1985**, *32*, 2657.
9. Chang, H. C.; Luo, Y. L.; Lin, K. C. *J. Chem. Phys.* **1991**, *94*, 3529.
10. Theodosiou, C. E. *Phys. Rev. A* **1984**, *30*, 2881.
11. Lindgaard, A; Nielsen, S. E. *At. Dat. Nucl. Data Tables* **1977**, *19*, 533.
12. Grudzev, P. F.; Denisov, V. I. *Opt. Spectrosc. (USSR)* **1982**, *52*, 8.
13. Breckenridge, W. H.; Umemoto, H. In *Dynamics of the Excited State*; Lawley, K. P., Ed.; Wiley: New York, **1982**; p 325.
14. Fabre, C.; Haroche, S. In *Rydberg States of Atoms and Molecules*; Stebbing, R. F.; Dunning, F. B., Eds.; Cambridge Univ.: Cambridge, **1983**; p 117.
15. Petitjean, L.; Gounand, F.; Fournier, P. R. *Phys. Rev. A* **1984**, *30*, 71.
16. Dubreuil, B.; Harnafi, M. *Phys. Rev. A* **1986**, *34*, 885.
17. Luo, Y. L.; Lin, K. C.; Liu, D. K.; Liu, H. J.; Luh, W. T. *Phys. Rev A* **1992**, in press.
18. Bauer, E.; Fisher, E. R.; Gilmore, F. R. *J. Chem. Phys.* **1969**, *51*, 4173.
19. Chang, M. L.; Huang J. T.; Lin, K. C. *J. Chin. Chem. Soc.* **1990**, *37*, 173.
20. Humphrey, L. M.; Gallagher, T. F.; Cooke, W. E.; Edelstein, S. A. *Phys. Rev. A* **1978**, *18*, 1383.
21. Gallagher, T. F.; Edelstein, S. A.; Hill, R. M. *Phys. Rev. Lett.* **1975**, *35*, 644.
22. Zare, R. N. *Ber. Bunsenges Phys. Chem.* **1982**, *86*, 422.
23. Leone, S. R. In *Selectivity in Chemical Reactions*; Whitehead, J. C., Ed.; Kluwer: Dordrecht, **1988**; p 245.
24. Hertel, I. V.; Schmidt, H.; Bahring, A.; Meyer, E. *Rep. Prog. Phys.* **1985**, *48*, 375.
25. Pouilly, B.; Alexander, M. H. *J. Chem. Phys.* **1987**, *86*, 4790.
26. Pouilly, B. *J. Chem. Phys.* **1991**, *95*, 5861.
27. Pouilly, B.; Robbe, J. M.; Alexander, M. H. *J. Chem. Phys.* **1989**, *91*, 1658.
28. Suits, A. G.; Hou, H.; Lee, Y. T. *J. Phys. Chem.* **1990**, *94*, 5672.
29. Hulser, H.; Campbell, E. E. B.; Witte, R.; Genger, H.; Hertel, I. V. *Phys. Rev. Lett.* **1990**, *64*, 392.
30. Wang, M. X.; de Vries, M. S.; Weiner, J. *Phys. Rev. A* **1986**, *33*, 765.
31. Manders, M. P. I.; van Hoek, W. B. M.; Vredenbregt, E. J. D.; Sandker, G. J.; Beijerinck, H. C. W.; Verhaar, B. J. *Phys. Rev. A* **1989**, *39*, 4467.
32. Bussert, W.; Neuschafer, D.; Leone, S. R. *J. Chem. Phys.* **1987**, *87*, 3833.
33. Lin, K. C.; Kleiber, P. D.; Wang, J. X., Stwalley, W. C.; Leone, S. R. *J. Chem. Phys.* **1988**, *89*, 4771.
34. Ananthamurthy, S.; Kleiber, P. D., Stwalley, W. C.; Lin, K. C. *J. Chem. Phys.* **1989**, *90*, 7605.
35. Breckenridge, W. H., *Acc. Chem. Res.* **1989**, *22*, 21.
36. Funk, D. J.; Breckenridge, W. H., *J. Chem. Phys.* **1989**, *90*, 2927.
37. Wallace, I.; Kaup, J.; Breckenridge, W. H., *J. Phys. Chem.* **1991**, *95*, 8060.
38. Duval, M. C.; Soep, B.; Breckenridge, W. H., *J. Phys. Chem.* **1991**, *95*, 7145.
39. Duh, Y. S.; Lin, K. C.; Luh, W. T., *Chem. Phys. Lett.* **1992**, *195*, 579.
40. Bussert, W.; Leone, S. R. *Chem. Phys. Lett.* **1987**, *138*, 269.
41. Lubman, D. M.; Rettner, C. T.; Zare, R. N. *J. Phys. Chem.* **1982**, *86*,1129.
42. Smalley, R. E., Wharton, L.; Levy, D. H. *Acc. Chem. Res.* **1977**, *10*, 139.
43. Miller, D. R. In *Atomic and Molecular Beam Methods*; Scoles, G., Ed.; Oxford Univ.: Oxford, **1988**; Vol. 1, p 14.
44. Breckenridge, W. H.; Umemoto, H. *J. Chem. Phys.* **1984**, *80*, 4168.
45. Kleiber, P. D.; Lyyra, A. M.; Sando, K. M.; Zafiropulos, S. V.; Stwalley, W. C. *J. Chem. Phys.* **1986**, *85*, 5493.
46. Kleiber, P. D.; Lyyra, A. M.; Sando, K. M.; Heneghan, S. P.; Stwalley, W. C. *Phys. Rev. Lett.* **1985**, *54*, 2003.
47. Breckenridge, W. H.; Wang, J. H. *Chem. Phys. Lett.* **1987**, *137*, 195.
48. Lin, K. C.; Huang, C. T. *J. Chem. Phys.* **1989**, *91*, 5387.
49. Hsiao, T. C.; Luo, Y. L.; Lin, K. C.; Luh, W. T. *J. Chin. Chem. Soc.* **1990**, *37*, 473.
50. Tsukiyama, K.; Katz, B; Bersohn, R. *J. Chem. Phys. 1985*, *83*, 2889.
51. Berry, M. J. *J. Chem. Phys.* **1973**, *59*, 6229.
52. Buss, R. J.; Casavecchia, P.; Hirooka, T.; Sibener, S. J.; Lee, Y. T. *Chem. Phys. Lett.* **1981**, *82*, 386.
53. Chaquin, P.; Sevin, A.; Yu, H. *J. Phys. Chem.* **1985**, *89*, 2813.
54. McCaffery, J. G.; Parnis, J. M.; Ozin, G. A.; Breckenridge, W. H. *J. Chem. Phys.* **1985**, *89*, 4945.
55. Rensberger, K. J.; Jeffries, J. B.; Crosley, D. R. *J. Chem. Phys.* **1989**, *90*, 2174.

56. Wang, K. C.; Lin, K. C.; Luh, W. T. *Chem. Phys. Lett.* **1992**, *188*, 37.
57. Brewer, P.; Das, P.; Ondrey, G.; Bersohn, R. *J. Chem. Phys.* **1983**, *79*, 720
58. Pence, W. H.; Baughcum, S. L.; Leone, S. R. *J. Phys. Chem.* **1981**, *85*, 3844.
59. Rose, T.; Rosker, M. J.; Zewail, A. H. *J. Chem. Phys.* **1989**, *91*, 7415.
60. Polanyi, J. C.; Schreiber, J. L. In *Physical chemistry-an advanced treatise*, Kinetics of gas reactions; Eyring, H.; Jost, W.; Henderson, D., Eds.; Academic Press: New York, **1974**; Vol. VIA, p 460.
61. Schilowitz, A. M.; Wiesenfeld, J. R. *J. Phys. Chem.* **1983**, *87*, 2194.
62. Lin, K. C.; Schilowitz, A. M.; Wiesenfeld, J. R. *J. Phys. Chem.* **1984**, *88*, 6670.
63. Wang, K. C.; Lin, K. C.; Luh, W. T. *J. Chem. Phys.* **1992**, *96*, 349.
64. Ke, C. B.; Chou, S. H.; Lin, K. C.; Luh, W. T. *J. Phys. Chem.* **1993**, in press.
65. Supronowicz, J.; Atkinson, J. B.; Krause, L. *Phys. Rev. A* **1985**, *31*, 2691.
66. Berends, R. W.; Kedzierski, W.; Krause, L. *J. Quant. Spectrosc. Radiat. Transfer* **1987**, *37*, 157.
67. Earl, B. L.; Herm, R. R. *J. Chem. Phys.* **1974**, *60*, 4568.
68. Orcutt, R. H.; Cole, R. H. *J. Chem. Phys.* **1967**, *46*, 697.
69. Nikitin, E. E. *J. Chem. Phys.* **1965**, *43*, 744.
70. Spielfiedel, A.; Gilbert, D.; Roueff, E.; Rostas, F. J. *Phys. B: Atom. Molec. Phys.* **1979**, *12*, 3693.